AIP | Journal of Applied Physics

The effect of millisecond flash lamp annealing on electrical and structural properties of ZnO:Al/Si structures

P. F. Lindberg, F. Lipp Bregolin, K. Wiesenhütter, U. Wiesenhütter, H. N. Riise, L. Vines, S. Prucnal, W. Skorupa, B. G. Svensson, and E. V. Monakhov

Citation: Journal of Applied Physics **119**, 185305 (2016); doi: 10.1063/1.4948666
View online: http://dx.doi.org/10.1063/1.4948666
View Table of Contents: http://scitation.aip.org/content/aip/journal/jap/119/18?ver=pdfcov
Published by the AIP Publishing

The effect of millisecond flash lamp annealing on electrical and structural properties of ZnO:Al/Si structures

P. F. Lindberg,[1] F. Lipp Bregolin,[2] K. Wiesenhütter,[2] U. Wiesenhütter,[2] H. N. Riise,[1] L. Vines,[1] S. Prucnal,[2] W. Skorupa,[2] B. G. Svensson,[1] and E. V. Monakhov[1]
[1]*Department of Physics, Centre for Materials Science and Nanotechnology, University of Oslo, P.O. Box 1048, Blindern, N-0316 Oslo, Norway*
[2]*Institute of Ion Beam Physics and Materials Research, Helmholtz-Zentrum Dresden-Rossendorf, P.O. Box 510119, 01314 Dresden, Germany*

(Received 24 February 2016; accepted 23 April 2016; published online 12 May 2016)

The effect of millisecond flash lamp annealing (FLA) on aluminum doped ZnO (AZO) films and their interface with Si have been studied. The AZO films were deposited by magnetron sputtering on Si (100) substrates. The electrical and structural properties of the film and AZO/Si structures were characterized by current–voltage, capacitance–voltage, and deep level transient spectroscopy measurements, X-ray diffraction, and secondary ion mass spectrometry. The resistivity of the AZO film is reduced to a close to state-of-the-art value of $2 \times 10^{-4}\,\Omega\,\mathrm{cm}$ after FLA for 3 ms with an average energy density of $29\,\mathrm{J/cm^2}$. In addition, most of the interfacial defects energy levels are simultaneously annealed out, except for one persisting shallow level, tentatively assigned to the vacancy-oxygen complex in Si, which was not affected by FLA. Subsequent to the FLA, the samples were treated in N_2 or forming gas (FG) (N_2/H_2, $90/10\%_{\mathrm{mole}}$) ambient at 200–500 °C. The latter samples maintained the low resistivity achieved after the FLA, but not the former ones. The interfacial defect level persisting after the FLA is removed by the FG treatment, concurrently as another level emerges at ~0.18 eV below the conduction band. The electrical data of the AZO films are discussed in term of point defects controlling the resistivity, and it is argued that the FLA promotes formation of electrically neutral clusters of Zink vacancies (V_{Zn}'s) rather than passivating/compensating complexes between the Al donors and V_{Zn}'s. *Published by AIP Publishing.* [http://dx.doi.org/10.1063/1.4948666]

I. INTRODUCTION

Transparent conductive oxides (TCO) are becoming a crucial part of state-of-the-art silicon-based solar cells and also of other optoelectronic devices. Indium tin oxide (ITO) is probably the most widely used TCO today, but the high cost and low abundance of indium drives the development of alternative TCOs based on low cost, abundant, and environmental-friendly materials. For instance, aluminum doped ZnO (AZO) appears as a promising candidate to replace the ITO based anti-reflective coating in Heterojunction with Intrinsic Thin layer (HIT) solar cell configurations, where the interface to the Si-layer plays an important role.[1] In this context, novel annealing techniques, such as flash lamp annealing (FLA), represent an exciting possibility to reduce the manufacturing cost of large area opto-electronic devices and also improve their performance.[2]

In order to substitute ITO with ZnO, equivalent or lower electrical resistivity of the film is required. There has been a substantial amount of work dedicated to reduce the resistivity of highly doped n-type ZnO films during the past decade and some groups have reported ZnO films with a resistivity less than $2 \times 10^{-4}\,\Omega\,\mathrm{cm}$.[3–6] The lowest resistivity films have been accomplished by Pulsed Laser Deposition (PLD) and Ga doping, yielding $\sim 8 \times 10^{-5}\,\Omega\,\mathrm{cm}$.[7] Unfortunately, PLD is not readily scalable to large area and high volume manufacturing, as compared with magnetron sputtering. Further, Al is far more abundant in the earth's crust than Ga and is preferable as a doping element for large scale TCO fabrication. So far, the lowest reported resistivity of sputter deposited AZO films is $\sim 1.1 \times 10^{-4}\,\Omega\,\mathrm{cm}$.[5]

FLA combines several intriguing possibilities, distinguishing the technique from Rapid Thermal Processing (RTP) and laser annealing. Full wafers can be exposed instantaneously, offering a great advantage over laser annealing. FLA enables annealing for a much shorter time ($\leq$1 ms) and at a higher power density than what is possible with RTP, hence making FLA well suited for in-line processing. Further, in this work, the highly non-equilibrium nature of FLA provides a mean to overcome thermodynamic constrains, such as dopant solubility, limiting more conventional annealing techniques.

The implementation of FLA in solar cell fabrication requires additional considerations, though: The structures must be resilient to the induced large temperature gradient, i.e., not subjectable to cracking.[8] In addition, FLA is proven to promote diffusion of dopants in Si.[9] Particularly regarding the HIT solar cell structure, thin amorphous layers subjected to FLA are reported to crystallize at an "explosive" rate when subjected to FLA.[10]

The FLA technique was initially developed for annealing of implantation-induced damage and electrical activation of dopants in silicon while minimizing diffusion (Refs. 11 and 12 and references therein). Recently, FLA has emerged as a viable technique for achieving highly conductive ZnO

films.[13] Gaspera *et al.*[14] demonstrated the applicability of FLA as a tool for post deposition annealing ZnO films fabricated by single step-chemical bath growth. By employing a series of 2 ms FLA pulses, low sheet resistivity ($40\,\Omega\,\square^{-1}$) of intrinsic ZnO films have been achieved, without subsequently heating the substrate. In addition, samples deposited on poly-ethylene terephthalate (PET) substrates, with very limited thermal stability, were also included in the work, demonstrating the selectivity of heating film over substrate by FLA. PET substrates have also been employed by Marjanovic *et al.*[15] for the fabrication of inkjet-printed electronics, requiring highly selective heating of the film over substrate, achieved by FLA for 10 ms at $10\,J/cm^2$. Gebel *et al.*[13] have studied the effect of FLA on AZO films deposited on glass substrates by magnetron sputtering at room temperature (RT). It was observed that FLA treatment for 1.2 ms reduced the resistivity by a factor of 2 down to $1.0 \times 10^{-3}\,\Omega\,cm$, suggesting that the FLA could substitute for the more conventional furnace and rapid thermal annealing (RTA) treatments.

FLA has also been explored for annealing of monocrystalline ZnO bulk samples doped by ion-implantation. Potzger *et al.*[16] employed FLA for annealing Fe-implanted samples with the intention to accomplish electrical activation with a minimum diffusion of Fe in order to avoid the formation of secondary magnetic phases. Potzger *et al.* discussed that crystalline ZnO is transparent to photons within the FLA energy spectrum and absorption by defects will prevail, hence promoting selective annealing of the damaged regions. The surface was recrystallized after annealing at energy densities equivalent to temperatures in the 1000–1100 °C range. Higher energy densities were required to remove the bulk damage, unfortunately, accompanied by a deterioration of the surface crystallinity. The non-equilibrium nature of FLA was also utilized by Børseth *et al.*[17] and Tuomisto[18] studying open volume defects, especially the zinc vacancy (V_{Zn}) and associated vacancy clusters, in ion-implanted ZnO bulk samples employing positron annihilation spectroscopy (PAS). V_{Zn} is a deep double acceptor with low formation energy in highly n-doped ZnO. It is, therefore, likely that a highly doped ZnO film will contain a high concentration of V_{Zn}-related defects after thermalization, reducing the effective carrier concentration. In addition, V_{Zn} is relatively mobile at low temperatures and forms readily stable complexes with shallow dopants, like Al, leading to dopant passivation/removal.[19] Clusters of $(V_{Zn})_n$ ($n \geq 3$), on the other hand, were found to be electrically neutral and also to act as traps for compensating residual impurities, like Li on substitutional site (Li_{Zn}). However, these $(V_{Zn})_n$ clusters have a rather limited thermal stability with a dissociation energy of ~2.6 eV and are challenging to form via thermodynamic equilibrium annealing techniques. Indeed, the $(V_{Zn})_n$ cluster formation is strongly promoted by FLA, in contrast to tube furnace and RTA treatments,[17] implying passivation/removal of shallow dopants through complexing with V_{Zn} is suppressed using FLA.

Evidently, FLA appears as an attractive technique for tailoring the concentration, clustering, and diffusion of V_{Zn}, which is of crucial importance for the implementation of heavily n-doped ZnO films as a high-performance TCO. However, reports on the use of FLA in conjunction with ZnO/Si structures, which are essential for Si-based photovoltaic devices, are scarce in the literature. Due to the differences in work function between AZO and moderately doped Si, a Schottky barrier is formed at the interface. The electrical characteristics of the ZnO/Si Schottky diode are indicative of the electronic quality of the junction and its interface. Because of the large lattice mismatch between AZO and Si, the junction is expected to be defect rich, but it has previously been proven that post deposition heat treatments can alter the interfacial defect energy distribution and concentration.[20] We have recently reported on the influence of the Si-substrate crystallographic orientation on the diode performance.[21,22] It was found that the substrate orientation influences the diode performance and defect distribution at the metallurgical junction. In addition, it was observed that a "soft" deposition technique, such as atomic layer deposition, yields a higher quality junction. However, irrespective of the growth method employed, an interfacial SiO_x layer occurs ($x \leq 2$). It exhibits an increasing thickness after post-deposition annealing using ordinary techniques and thus prevents an optimal electrical contact between the AZO layer and the Si substrate.[23]

In this work, we report on the effect of FLA and subsequent heat treatments on AZO/Si(100) structures. In contrast to Ref. 13, where the AZO films were deposited on glass substrates and the heating originated from the poorly absorbing AZO films, the heating of our samples originates from absorption in the underlying Si substrate. We demonstrate that the resistivity (ρ) of the as-deposited AZO films can be decreased down to state-of-the-art values by FLA. It is also shown that post-FLA heat treatment does not further reduce the resistivity. It is argued that there are different types of point defects limiting the conductivity of the AZO films, such as complexes between Al_{Zn} and V_{Zn}, and that their combination is suppressed by FLA while forming electrically neutral clusters of $(V_{Zn})_n$ ($n \geq 3$). Additionally, the density of interface states in the AZO/Si(100) structures, prepared by magnetron sputtering, decreases after the FLA. However, one prominent defect level, located at ~0.17 eV below the conduction band edge (E_C), persists, but disappears after post FLA treatment in forming gas (FG) (N_2/H_2, $90/10\%_{mole}$) ambient, albeit accompanied by the growth of another level at 0.18 eV below E_C. The identity of the defects responsible for the two levels is discussed, and the former one is tentatively assigned to the vacancy-oxygen center (VO) on the Si side of the AZO/Si interface. The latter one may possibly be associated with a high-order vacancy-oxygen complex involving hydrogen.

II. EXPERIMENTAL DETAILS

AZO films, 180 nm thick, were deposited by RF and DC co-sputtering of ZnO and Al at 400 °C on n-type Si(100) float zone (FZ) and Czochralski (Cz) wafers with resistivities of 4–5 kΩ cm and 3–10 Ω cm, respectively. Before deposition of the AZO film, the substrates were cleaned by a standard RCA-rinsing procedure. Immediately prior to loading the

substrates into the deposition chamber, they were HF-dipped and blow-dried with N_2. The AZO film deposition was performed using a Semicore Triaxis RF/DC Magnetron Sputter system with a sintered ceramic ZnO target and a metallic Al target, 99.999% and 99.99% purity, respectively. The resulting film thickness was measured by both ellipsometry and surface stylus profilometry. After the deposition, the wafers were cut into samples with a size of $10 \times 10\,mm^2$.

The FLA system used is based on low pressure Xenon filled flash lamps coupled to a capacitor bank. The FLA treatments were performed in Ar atmosphere and the system is described in Ref. 12. A survey of the studied samples is given in Table I. The samples B1–B5 were subjected to FLA with energy densities in the range of 26–41 J/cm^2 for a duration of 3 ms with no further treatment.

The samples C1–C4 and D1–D4, having a similar high-resistivity substrate as the B samples, were exposed to an FLA density of 31 J/cm^2 only (3 ms duration) and then post FLA treated in a tube furnace for 30 min at 200–500 °C using either N_2 or FG flow (>2 l/min). The samples E2–E4, having a "medium" resistivity substrate of $\sim 6 \pm 3\,\Omega$ cm, were also subjected to FLA density of 31 J/cm^2 followed by no further treatment or furnace annealing at 500 °C in N_2 or FG flow. All the C1–C4, D1–D4, and E2–E4 were treated during the same FLA run.

Subsequently, mesa-diodes were prepared using the samples E1–E4. The AZO film was covered by a photoresist lift-off mask and thereafter the whole front side of the samples was covered by an e-beam evaporated Al film. After the Al deposition, the photoresist was dissolved in acetone in an ultrasonic bath leaving 1.35 mm in diameter circular Al front side contacts on the AZO film. The exposed AZO was etched-back in a solution of $C_2H_4O_2$:H_3PO_4:H_2O, 1:1:60, using the Al front side contact as an etch stop, without the requirement of a second photolithography step. The back side of the Si substrate was contacted by applying an In-Ga eutectic alloy.

TABLE I. Survey of samples used.

Sample	Substrate ρ (Ω cm)	FLA (J/cm^2)	Post FLA ann. (°C)
A1	4–5 k	…	…
B1	4–5 k	26	…
B2	4–5 k	29	…
B3	4–5 k	33	…
B4	4–5 k	37	…
B5	4–5 k	41	…
C1	4–5 k	31	200 N_2
C2	4–5 k	31	300 N_2
C3	4–5 k	31	400 N_2
C4	4–5 k	31	500 N_2
D1	4–5 k	31	200 FG
D2	4–5 k	31	300 FG
D3	4–5 k	31	400 FG
D4	4–5 k	31	500 FG
E1	3–10	…	…
E2	3–10	31	…
E3	3–10	31	500 N_2
E4	3–10	31	500 FG

Structural analysis of the films deposited on the high resistivity substrate was performed using a Bruker AXS D8 Discover X-ray diffraction system (XRD), encompassing a θ-2θ survey scan ranging from 20° to 80° and a high resolution scan between 34° and 36° enveloping the (0002) reflection of ZnO.

Hall effect measurements were conducted at room temperature (RT) using a setup composed of a Keithley 7001 channel controller, Keithley 2182 voltmeter, and a Keithley 6221current source. The samples were contacted by gold covered metal springs in a van der Pauw configuration. Current–voltage (IV) measurements were carried out using a Keithley 6487 picoammeter/voltage source. All the IV measurements were performed in darkness and at RT. The same holds for the capacitance-versus-voltage measurement (CV) using a Boonton 7200 meter (1 MHz probe frequency).

Deep level transient spectroscopy (DLTS) was undertaken in the temperature range 50–300 K using a refined version of the setup described in Ref. 24. The DLTS spectra were extracted using a lock-in weighting function and employing six different rate widows, ranging from $(20\,ms)^{-1}$ to $(640\,ms)^{-1}$, recorded simultaneously during one temperature scan.

Secondary Ion Mass Spectrometry (SIMS) analysis was performed using a Cameca IMS 7F magnetic sector instrument. A 10 keV O_2 primary beam was rastered over an area of $200 \times 200\,\mu m^2$, and positive secondary ions emitted from the central part (62 μm in diameter) of the sputtered crater were recorded. A constant erosion rate was assumed for depth calibration and the crater depths were measured by surface stylus profilometry. Implanted reference samples were used to convert the Al, Si, and H signal into impurity concentrations, while the detection limit for H was estimated to be $\sim 10^{18}\,cm^{-3}$.[25]

III. RESULTS AND DISCUSSION

The AZO films exhibit preferential growth along the c-axis with no secondary phases observed after deposition (Fig. 1(a)).

The high resolution data in Fig. 1(b) reveal how the (0002) peak evolves with the FLA energy density; at 26 J/cm^2, the peak intensity increases significantly and the position shifts slightly to a lower angle. At and above 29 J/cm^2, the peak shifts to higher θ-2θ angles, indicating a compression along the c-axis. A similar shift has been reported by Tong *et al.* and was attributed to the substitution of Zn with Al in the ZnO lattice.[26] After 37 and 41 J/cm^2, a weak reflection emerges at 35.44°. The reflection cannot be unambiguously assigned to any phase consisting of the elements Zn, Al, Si, or O, listed in standard power diffraction, ICDD, cards. One can speculate that it can be a ZnO $(10\bar{1}1)$[27,28] or Al_2O_3 (104) reflection at 36.25° or 35.15°. The latter can be theoreticized to be due to Al segregation.

The most abundant impurities in the AZO films have been identified by SIMS as Al and H, rather homogenously distributed to a depth of ~140 nm before matrix effects from the AZO/Si interface start to affect the secondary ion field[29] (Figs. 2(c) and 2(d)). The H content is in the $10^{18}\,cm^{-3}$

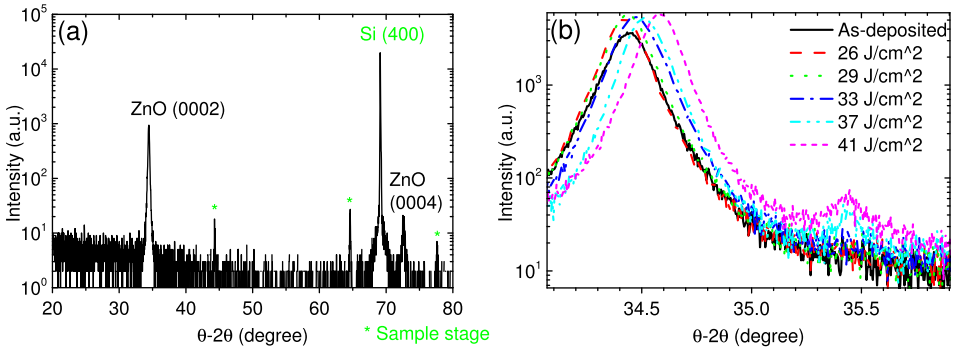

FIG. 1. (a) θ-2θ scan of as-deposited AZO film; sample A1. (b) High resolution scan of the (0002) reflection in films treated by FLA 3 ms pulses with energy densities up to 41 J/cm^2; samples A1 and B1–B5.

range, unintentionally introduced during sputter deposition, but still about two orders of magnitude below that of Al and the latter appear as the clearly dominating shallow donor impurity. All other elements are estimated to be in the 10^{17} cm^{-3} range or below, in agreement with preceding studies.[30]

In addition to identifying the main impurities, the SIMS results give also an indication of the extension and abruptness of the interfacial region. For energy densities $\lesssim$33 J/cm^2 the Si signal in Fig. 2(b) increases by more than four orders of magnitude over a 20 nm interval, indicative of an abrupt interface. FLA at $\gtrsim$37 J/cm^2 causes in-diffusion of Si into the AZO film. A similar redistribution is also obtained for O (data not shown) and Al, suggesting a broadening of the interfacial region. Also, Zn redistributes after the FLA at 37 J/cm^2 (Fig. 2(a)), and the width of the Zn peak after 41 J/cm^2 is similar to that of the Si peak. Hydrogen is present already in the as-deposited AZO film, with Fig. 2(d) evidencing incorporation during the growth. After the FLA at 33 J/cm^2 the H signal is reduced and at higher energy densities a slight redistribution occurs with a pronounced peak in the interfacial region. However, the H concentration remains about two orders of magnitude below that of Al (Fig. 2(c)).

In general, both the XRD data in Fig. 1 and the SIMS data in Fig. 2 show that the AZO/Si structures are rather stable for FLA energy densities below 33 J/cm^2, with no

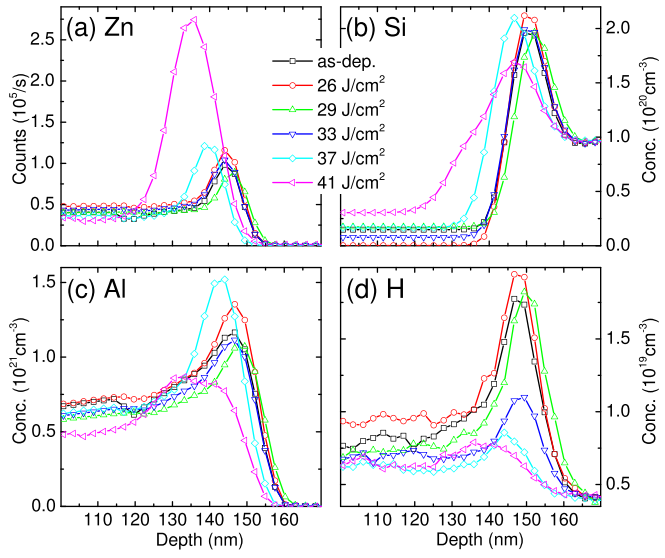

FIG. 2. Depth profiles of Zn (a), Si (b), Al (c), and H (d) as measured by SIMS after FLA treatments with different energy density.

detection of secondary phases and a rather abrupt interface. Accordingly, the samples C1–C4, D1–D4, and E2–E4, subjected to an FLA density of 31 J/cm^2, and primarily used for the electrical characterization, are anticipated to have well-preserved AZO/Si structures.

The resistivity (ρ), Hall mobility (μ), and net electron concentration (n) values for the AZO films of the samples A1, B1–B5, C1–C4, and D1–D4 have been deduced from RT Hall-effect measurements, as displayed in Fig. 3. The high resistivity Si substrate used (4–5 kΩ cm) yielded a negligible contribution to the deduced values.

Fig. 3(a) shows the evolution of ρ, μ, and n as a function of the FLA energy density (pulse duration 3 ms). The lowest ρ value reached is 2.1×10^{-4} Ω cm and occurs at 29 J/cm^2. The reduction in ρ is about a factor of 3 relative to the as-deposited film. The decrease is due to an almost equal relative increase in both n (from $\sim 5.3 \times 10^{20}$ to $\sim 9 \times 10^{20}$ cm^{-3}) and μ (from $\sim$21 to $\sim$34 cm^2/V s). For energy densities above $\sim$29 J/cm^2, the electron concentration decreases gradually while μ continues to increase until $\sim$37 J/cm^2, resulting in a weak increase of ρ.

The increase in n with the FLA-density up to 29 J/cm^2 is likely due to an increased fraction of activated shallow Al donors and a larger amount of electrically inactive $(V_{Zn})_n$ clusters. The following decrease in n at higher densities may be attributed to passivation of the Al dopants by the formation of complexes with V_{Zn} (Al-V_{Zn}) and ($2Al_{Zn}$-V_{Zn}),[19,31] rather than to compensation by isolated V_{Zn}'s.[32] The V_{Zn}'s are mobile at rather moderate temperatures and readily form complexes with shallow n-type dopants.[19,36] In fact, electron paramagnetic resonance measurements have shown that the (Al-V_{Zn}) complexes are energetically favorable and act as a deep acceptor with the energy level located $\sim$1 eV above the valence band edge.[19] Thus, the (Al-V_{Zn}) complex literally removes the shallow Al donor and also acts as a deep compensating defect, while the ($2Al_{Zn}$-V_{Zn}) complex is electrically neutral. The dominating scattering mechanisms in heavily doped, poly crystalline AZO films are usually considered to be grain boundary and ionized donor impurity scattering.[33] Pei *et al.* argue that grain boundary scattering dominates only if the grain size is significantly smaller than the mean free path (λ) of the electrons. In our samples, the value of λ has been estimated to be $\sim$7 nm using the relation[34]

$$\lambda = \mu \frac{h}{e} \left(\frac{3}{8\pi} n \right)^{1/3}, \quad (1)$$

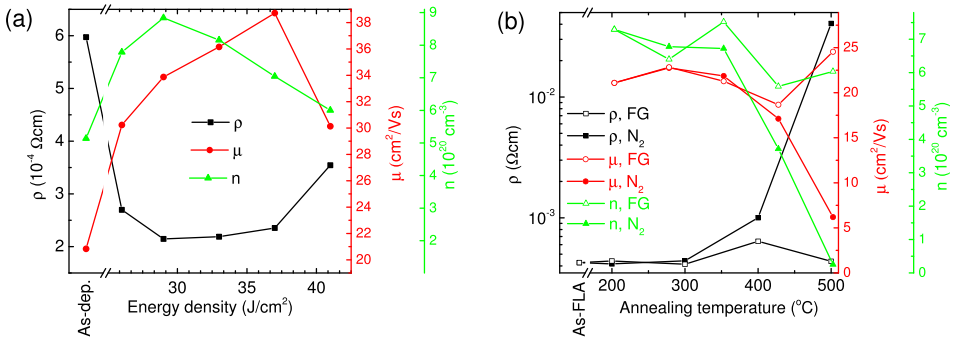

FIG. 3. (a) Resistivity (ρ), mobility (μ), and carrier concentration (n) of samples A1 and B1–B5, deduced from Hall effect measurements. (b) Hall effect measurements of samples C1–C4 and D1–D4.

where h is the Planck's constant and e is the elementary charge. The calculated λ value is significantly smaller than the average crystallite size (~20 nm), and therefore, the dominating scattering is attributed to ionized donors. Hence, μ is expected to increase with the removal/passivation of ionized dopants,[35,36] both the (Al_{Zn}-V_{Zn}) and ($2Al_{Zn}$-V_{Zn}) complexes will reduce n and simultaneously suppress the importance of ionized impurity scattering relative to that of separately ionized scattered constituents, i.e., Al_{Zn}^{+} and V_{Zn}^{2-}. Indeed, the data in Fig. 3(a) corroborate the conclusion that compensation by isolated V_{Zn}'s plays a minor role since it cannot account for the simultaneous decrease in n and increase in μ.

On the basis of the results in Fig. 3(a), together with the XRD and SIMS data, 31 J/cm^2 was determined as the optimum FLA parameter for enhancing the conductivity and crystallinity, while simultaneously minimizing diffusion, of the AZO/Si structures. Therefore, the samples C1–C4, D1–D4, and E2–E4 were FLA treated at 31 J/cm^2. The evolution of ρ, μ, and n for the C1–C4 and D1–D4 samples, post-FLA treated in N_2 or FG ambients, respectively, is shown in Fig. 3(b). The resistivity of the C1–C4 films increases with the treatment temperature and more than doubles after 400 °C. Annealing at 500 °C causes an increase in ρ by two orders of magnitude, as compared with the as-FLA sample. In contrast, the ρ for the samples D1–D4 remains low up to maximum temperature used with only minor variation in both μ and n. The drastic increase in ρ for the C samples after the 500 °C annealing is due to a decrease in both μ and n, where μ drops by a factor of 3 and n by more than one order of magnitude. The decrease in both μ and n implies that compensation by deep-level acceptors is the dominant process and not passivation/removal shallow donors. As already discussed, the latter process leads to an increase in μ because of less ionized impurity—scattering. During the post FLA-treatment, thermodynamic equilibrium starts to apply and the neutral $(V_{Zn})_n$ clusters, promoted by the non-equilibrium FLA, will gradually dissolve.[17] Accordingly, formation of the deep (Al_{Zn}-V_{Zn}) acceptor becomes more pronounced, giving rise to charge carrier compensation as well as actual removal of the Al_{Zn} donor.[19] In the D samples, passivation of the released V_{Zn}'s by in-diffusion of H atoms from the FG ambient appears to prevail,[37] and ρ, n, and μ stay unchanged.

The IV characteristics of the samples E1–E4 are given in Fig. 4(a). Sample E1 (as-deposited AZO film) shows a Schottky-type behavior with a current rectification of almost five orders of magnitude, between −1 and 1 V, and an ideality factor of 2.2.

After the FLA (sample E2), the forward current is less limited by series resistance, as compared with E1, and the ideality factor is reduced to 1.8 while the reverse bias current is increased. The sample E3 (post FLA treatment in N_2) exhibits an overall lower current than E2 and a significantly higher ideality factor; 2.4. The E4 sample (post FLA treated in FG) features the largest current rectification and lowest ideality factor among all the samples; 1.7. The ideality factor scales with the generation-recombination current component (GR) and can be corroborated to the concentration of interfacial defects, as will be shown from DLTS measurements, Fig. 5, indicating that a large concentration of interfacial energy levels results in a larger ideality factor. In analogy with a metal/semiconductor junction, the Schottky–Mott model[38] is, in a first approximation, applied to describe the current characteristics of the samples where the barrier height, Φ_b, is given by the relation

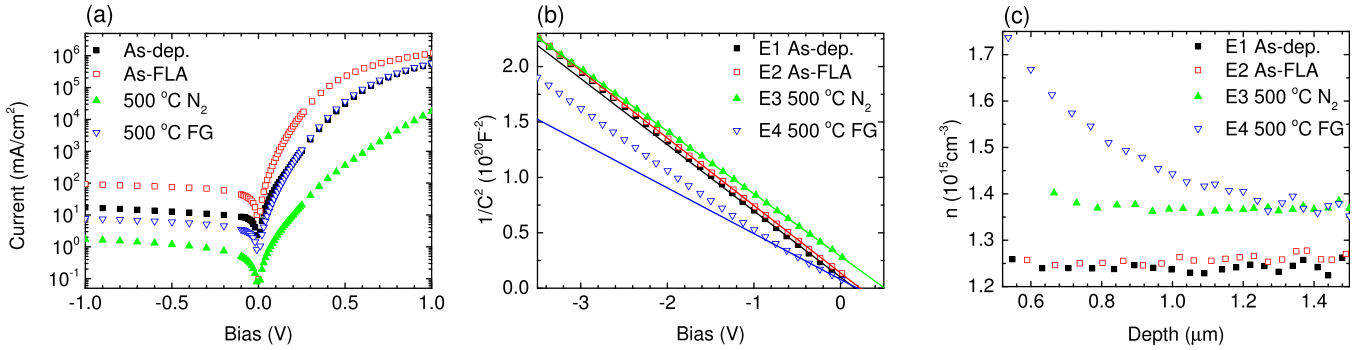

FIG. 4. IV (a) and CV (b) characteristics of samples E1–E4. (c) Electron concentration as a function of depth, deduced from (b).

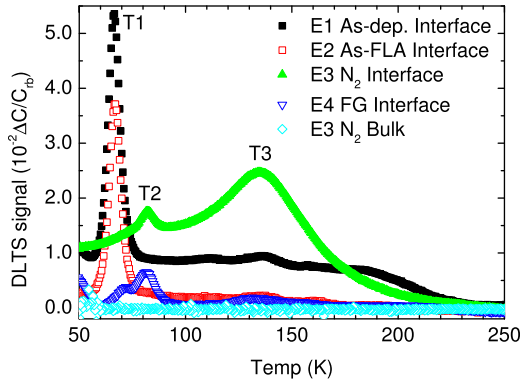

FIG. 5. DLTS spectra of the samples E1–E4, rate window $(640\,\text{ms})^{-1}$.

$$\Phi_b^{IV} = kT \times \ln(A^* A T^2 / I_o), \tag{2}$$

where k is the Boltzmann's constant, A^* is the Richardson constant, A is the contact area, T is the absolute temperature, and I_o is dark saturation current, deduced from extrapolating the straight line of ln(I) to $V = 0$. The Φ_b^{IV} values deduced, 0.4, 0.3, 0.5, and 0.4 eV for the samples E1–E4, respectively, are significantly lower than the literature values for samples prepared by ALD and display atomically sharp interfaces; 0.65 eV.[22] The low barrier height is indicative of a defect rich interface, causing trap assisted electron tunneling.[39]

The reverse bias capacitance, C, plotted in Fig. 4(b) as C^{-2} versus the reverse bias voltage V, follows a close to linear behavior for the samples E1, E2, and E3. E3 is distinguished by a larger built in voltage than the other samples, which can be attributed to a high density of interfacial electron traps, as will be discussed later in conjunction with the DLTS data in Fig. 5. It is, therefore, expected that the Fermi level position is pinned at the interface, causing an apparent larger built in voltage and barrier height, as compared with the other samples. The net doping concentrations versus depth profiles, extracted from the data in Fig. 4(b), are depicted in Fig. 4(c). Except for the near interfacial region of sample E4, the profiles are rather uniform with an absolute value of $\sim 1.3 \times 10^{15}$ or $\sim 1.4 \times 10^{15}\,\text{cm}^{-3}$, where the latter one holds for the post FLA treated samples (E3 and E4). The increase in net doping for sample E3 in the vicinity of the AZO/Si interface is attributed to the presence of H during the FG annealing. Substantial concentrations of so-called thermal donors (TD) ($\sim 10^{16}\,\text{cm}^{-3}$ after 100 h, 450 °C annealing[43]) occur in Czochralski-grown (Cz) Si wafers subjected to annealing in the range of 300–500 °C.[40] The TDs arise from defects complexes involving oxygen, the main residual impurity in Cz-Si, and their formation rate hinges on the diffusivity of various O-species, e.g., interstitial O atoms and O_2 dimers.[41,42] It is well established that H promotes the diffusivity of O-species[43] and an enhancement of the electron carrier concentration caused by TDs after annealing in FG at 500 °C is indeed anticipated.

Defect levels present in the AZO/Si heterojunctions have been characterized by DLTS, and the results are shown in Fig. 5. Here, it should be pointed out that the depletion region extends almost exclusively on the Si side of the heterojunction because of the large difference in carrier concentration, $\sim 10^{20}\,\text{cm}^{-3}$ in the AZO film and $\sim 10^{15}\,\text{cm}^{-3}$ in the Si substrate. Hence, the defect levels observed in Fig. 5 are predominately situated on the Si side of the junction. Further, using a significantly larger reverse bias voltage than the filling pulse one in the DLTS measurements, contributions from traps situated close to the AZO/Si interface are excluded.

Thus, the bulk of the Si substrate was probed by applying −1.5 V as reverse bias voltage with a filling pulse of 1 V (1 s duration), i.e., the total charging voltage was −0.5 V. As illustrated in Fig. 5, for the E3 sample, no defect levels were detected in the Si bulk, with concentrations above the detection limit ($\sim 5 \times 10^{10}\,\text{cm}^{-3}$).

In contrast, a considerable density of interfacial defect levels were observed by applying −1 V in reverse bias voltage and 2 V in filling pulse, ensuring filling of the interfacial traps. The E1 sample displays one distinct peak, labeled T1, in addition to a broad band of defect levels. It is speculated that the rather homogeneously distributed background signal in the as-grown sample E1 is due to strained Si-Si bonds at the surface toward the SiO_2 layer, which is commonly observed as a U-shaped distribution of states in Si/SiO_2 structures.[44–46] The T1 peak maximum occurs at 67 K in Fig. 5 (rate window $= (640\,\text{ms})^{-1}$) and undertaking an Arrhenius analysis by utilizing the data from all the six rate windows recorded a level position of ∼0.17 eV below the E_C with an apparent capture cross section of $1.2 \times 10^{-12}\,\text{cm}^2$. After the FLA, the broad defect band has disappeared to a large extent, while T1 remains, though somewhat reduced in intensity.

Post FLA treatment in N_2 ambient (sample E3) introduces a high concentration of interfacial traps distributed over a wide energy (temperature) range, labeled T3. The T3 peak cannot be accurately fitted to one single energy level, and is therefore concluded to be constituted of an energy band. The T1 peak is not distinguishable in the E3 sample, whereas a new peak introduced at 82 K, labeled T2, and positioned at $\sim E_C$–0.18 eV with an apparent capture cross section of $1.2 \times 10^{-14}\,\text{cm}^2$ is obtained. The E4 sample, on the other hand, shows a very low concentration of interfacial deep defect levels, even below that of the E2 sample, but a fraction of T1 remains and concurrently the T2 peak occurs, similar to that in the E3 sample.

The improved IV characteristics, with a low ideality factor and high rectification, of the E4 sample (Fig. 4(a)) correlates with the disappearance of the broad energy band T3 in Fig. 5. These traps are likely to act as recombination centers, increasing the ideality factor, and also to pin the Fermi level leading to an apparent high barrier height for the E3 sample (cf. Fig. 4(b)). The identity of these traps is not known but it can be speculated that they arise from defects of dangling bond character, such as the Pb_1 defect.[47] Such defects are known to interact strongly with H in silicon, being electrically passivated,[48] and this would account for their suppression in the E4 sample (treated in FG).

An increase in electron concentration is observed for samples E3 and E4, and it is speculated that it is due to TDs (cf. Fig. 4(c)). The (++/+) charge state transition for TD species depends on the exact atomic configuration and is around ∼0.14 eV below E_C.[49,50] This implies that T2 is too

deep to be associated with possible TDs giving rise to the increase in n. Further, the position of T2 does not vary with the electric field in the probed region, and no evidence of a Poole–Frenkel effect is found, which rules out the donor-like nature of the center. In addition, the estimated concentration of T2 is more than one order of magnitude below the increase in n. Evidence for shallow donor states are found, but they appear very close to freeze-out in the DLTS spectra and no accurate evaluation of their energy positions or concentration can be made.

The presence of defects with dangling bonds, like vacancy-related complexes, at the AZO/Si interface may be further corroborated by the T1 and T2 levels. They are both located relatively shallow in the bandgap and primarily affect the current transport over the AZO/Si interface via electron trapping, rather than carrier recombination. T1 is tentatively ascribed to the prominent vacancy-oxygen center (VO) in the Cz-Si, having a state at $\sim E_C$–0.17 eV.[51] The VO center is one of the most extensively studied point defects in O-rich Si and it starts typically to anneal out at temperature above ~300 °C, where the exact kinetics depends on the concentration of interstitial O-atoms and other impurities, like H and C.[52] Hence, both the energy position and the thermal stability of the T1 defect are consistent with those of the VO center. However, in hydrogenated and diffusion-oxygenated float zone Si (DOFZ) Si wafers, the loss of the VO center at 400 °C is accompanied by the growth of the so-called E7 peak.[53] E7 occurs on the high-temperature tail on the VO peak in the DLTS spectra after annealing, similar to that of T2 in Fig. 5, and it appears likely that T2 is identical to E7. The identity of the E7 level is not known but it is only observed in samples with a high concentration of both H and O,[53] consistent with T2 being most pronounced in the E4 sample (treated in FG). In addition, also the AZO films contain substantial concentration of H (Fig. 2(d)), with a tendency of being released at temperatures of ~500 °C.[54]

It should be pointed out that an extensive study on the identification of the observed DLTS peaks is out of the scope of the present investigation, and further studies are needed to substantiate these speculations on the nature of the observed complexes.

IV. SUMMARY AND CONCLUSION

We have studied the effect of millisecond FLA on the structural and electronic properties of AZO films deposited by magnetron sputtering on n-type Si(100) samples. The resistivity of the films exhibited a close to state-of-the-art value of $2 \times 10^{-4}\,\Omega$ cm using an FLA energy density of 29 J/cm^2. It is argued that the highly non-equilibrium FLA promotes formation of electrically inactive $(V_{Zn})_n$ clusters rather than formation of passivating/compensating complexes between Al_{Zn} and V_{Zn}. This enhances both n (Al_{Zn} activation) and μ in the AZO films. In addition, the concentration of deep defect states at the AZO/Si interface is simultaneously substantially reduced by the FLA. For FLA densities above 29 J/cm^2, the ρ increases with a loss in n while μ increases somewhat, indicating that passivation of the Al_{Zn} donors occurs. Post-FLA furnace treatment at 500 °C in FG has no effect on the ρ while a corresponding treatment in N_2 ambient increases ρ by two orders of magnitude. This drastic increase in ρ is due to the compensation of the Al_{Zn} donors by deep level acceptors, presumably (Al_{Zn}-V_{Zn}) centers formed when V_{Zn}'s are dissolved from the $(V_{Zn})_n$ cluster. In the FG treated samples, the (Al_{Zn}-V_{Zn}) centers are efficiently passivated by in-diffusing H-atoms yielding no net effect in ρ, n, and μ. Evidence for the beneficial effect of H is also found for the defect states at the AZO/Si interface, where post-FLA FG-treatment strongly suppresses the concentration of shallow electron traps without giving rise to the deep bandgap states observed post-FLA N_2-treatment. The resulting AZO/Si heterojunctions after the post-FLA FG-treatment displayed a current rectification by about five orders of magnitude with an ideality factor of ~1.7 and barrier height of ~0.5 eV. In conclusion, FLA followed by FG-treatment appears, indeed, as a promising concept to accomplish low-resistivity AZO films and integrate them in a low-temperature Si-processing sequence for solar cells.

ACKNOWLEDGMENTS

This work was performed within "The Norwegian Research Centre for Solar Cell Technology" (Project No. 193829); a Centre for Environment-friendly Energy Research, co-sponsored by the Norwegian Research Council, research and industry partners in Norway. Travel grants have been funded by the German Academic Exchange Service (DAAD) and the Norwegian research council.

[1]M. Tanaka, M. Taguchi, and T. Matsuyama, Jpn. J. Appl. Phys., Part 1 **31**, 3518 (1992).
[2]S. Prucnal, T. Shumann, W. Skorupa, B. Abendroth, K. Krockert, and H. J. Müller, Acta Phys. Pol., A **120**, 30 (2011).
[3]T. Minami, Semicond. Sci. Technol. **20**, S35 (2005).
[4]H. Agura, A. Suzuki, T. Matsushita, T. Aoki, and M. Okuda, Thin Solid Films **445**, 263 (2003).
[5]X.-R. Deng, H. Deng, M. Wei, and J.-J. Chen, J. Mater. Sci.: Mater. Electron. **23**, 413 (2012).
[6]D. C. Look, T. C. Droubay, and S. A. Chamber, Appl. Phys. Lett. **101**, 102101 (2012).
[7]S.-M. Park, T. Ikegami, and K. Ebihara, Thin Solid Films **513**, 90 (2006).
[8]Y. Wang, S. Chen, X. Wang, and M. Shen, in 20th International Conference on Ion Implantation Technology (IIT) (2014).
[9]H. B. Normann, L. Vines, V. Privitera, W. Skorupa, T. Schumann, B. G. Svensson, and E. V. Monakhov, Appl. Phys. Lett. **102**, 132108 (2013).
[10]K. Ohdaira, T. Fujiwara, Y. Endo, S. Nishizaki, and H. Matsumura, J. Appl Phys. **106**, 044907 (2009).
[11]W. Skorupa, R. A. Yankov, M. Voelskow, W. Anwand, D. Panknin, R. A. McMahon, M. Smith, T. Gebel, L. Rebohle, R. Fendler, and W. Hensch, in *Proceedings of 13th IEEE International Conference on Advanced Thermal Processing of Semiconductors - RTP-2005, Santa Barbara, October 04–07* (2005), p. 53.
[12]W. Skorupa, T. Gebel, R. A. Yankov, S. Paul, W. Lerch, D. F. Downey, and E. A. Arevalo, J. Electrochem. Soc. **152**, G436 (2005).
[13]T. Gebel, M. Neubert, R. Endler, J. Weber, M. Vinnichenko, A. Kolitsch, W. Skorupa, and H. Liepack, MRS Symp. Proc. **1287**, f10-10 (2011).
[14]E. D. Gaspera, D. F. Kennedy, J. van Embden, A. S. R. Chesman, T. R. Gengenbach, K. Weber, and J. J. Jasieniak, Adv. Funct. Mater. **25**, 7263 (2015).
[15]N. Marjanovic, J. Hammerschmidt, J. Perelaer, S. Farnsworth, I. Rawson, M. Kus, E. Yenel, S. Tilki, U. S. Schubert, and R. R. Baumann, J. Mater. Chem. **21**, 13634 (2011).
[16]K. Potzger, W. Anwand, H. Reuther, S. Zhou, G. Talut, G. Brauer, W. Skorupa, and J. Fassbender, J. Appl. Phys. **101**, 033906 (2007).

[17]T. M. Børseth, F. Tuomisto, J. S. Christensen, W. Skorupa, E. V. Monakhov, B. G. Svensson, and A. Y. Kuznetsov, Phys. Rev. B **74**, 161202 (2006).
[18]F. Tuomisto, Appl. Surf. Sci. **255**, 54 (2008).
[19]J. E. Stehr, K. M. Johansen, T. S. Bjørheim, L. Vines, B. G. Svensson, W. M. Chen, and I. A. Buyanova, Phys. Rev. B **2**, 021001 (2014).
[20]L. J. Brillson, B. G. Svensson, S. J. Perton, and C. Jagadish, *Oxide Semiconductors* (Elsevier, San Diego, 2013), pp.105–157.
[21]P. Lindberg, V. Quemener, K. Bergum, J. Gan, B. G. Svensson, and E. V. Monakhov, MRS Proc. **1699** (2014).
[22]V. Quemener, L. Vines, E. V. Monakhov, and B. G. Svensson, Thin Solid Films **519**, 5763 (2011).
[23]J. Škriniarová, J. Kovác, D. Haško, A. Vincze, J. Jakabovic, L. Jánoš, M. Veselý, I. Novotný, and J. Bruncko, J. Phys.: Conf. Ser. **100**, 042031 (2008).
[24]B. G. Svensson, K. H. Rydén, and B. M. S. Lewerentz, J. Appl. Phys. **66**, 1699 (1989).
[25]L. Vines and A. Y. Kuznetsov, in *Semiconductors and Semimetals/Oxide Semiconductors*, edited by B. G. Svensson, S. J. Pearton, and C. Jagadish (Elsevier/AP, New York, 2013).
[26]H. Tong, Z. Deng, Z. Liu, C. Huang, J. Huang, H. Lan, C. Wang, and Y. Cao, Appl. Surf. Sci. **257**, 4906 (2011).
[27]H.-S. Chin and L.-S. Chao, J. Nanomater. **2013**, 424953 (2013).
[28]J. Sengupta, R. K. Sahoo, and C. D. Mukherjee, Mater. Lett. **83**, 84 (2012).
[29]H. Malmbekk, L. Vines, E. V. Monakhov, and B. G. Svensson, J. Appl. Phys. **110**, 074503 (2011).
[30]R. Schifano, M. Schofield, L. Vines, S. Diplas, E. V. Monakhov, and B. G. Svensson, IOP Conf. Ser.: Mater. Sci. Eng. **34**, 012007 (2012).
[31]J. T-Thienprasert, S. Rujirawat, W. Klysubun, J. N. Duenow, T. J. Coutts, S. B. Zhang, D. C. Look, and S. Limpijumnong, Phys. Rev. Lett. **110**, 055502 (2013).
[32]D. C. Look, K. D. Leedy, L. Vines, B. G. Svensson, A. Zubiaga, F. Tuomisto, D. R. Doutt, and L. J. Brillson, Phys. Rev. B **84**, 115202 (2011).
[33]Z. L. Pei, C. Sun, M. H. Tan, J. Q. Xiao, D. H. Guan, R. F. Huang, and L. S. Wen, J. Appl. Phys. **90**, 3432 (2001).
[34]L. Eckertova, *Physics of Thin Films* (Plenum Press, New York, 1977), p. 180.
[35]J. R. Bellingham, W. A. Phillips, and C. J. Adkins, J. Mater. Sci. Lett. **11**, 263 (1992).
[36]L. S. Sheng and R. W. Thurber, Solid-State Electron. **20**, 609 (1977).
[37]M. G. Wardle, J. P. Goss, and P. R. Briddon, Phys. Rev. B **72**, 155108 (2005).
[38]S. M. Sze and K. N. Kwok, *Physics of Semiconductor Devices* (John Wiley & Sons, New Jersey, 2006), pp. 393–395.
[39]T. Serin, S. Gürakar, N. Serin, N. Yıldırım, and F. Kuş Özyurt, J. Phys. D: Appl. Phys. **42**, 225108 (2009).
[40]A. Ourmazd, W. Schröter, and A. Bourret, J. Appl. Phys. **56**, 1670 (1984).
[41]S. K. Estreicher, Phys. Rev. B **41**, 9886 (1990).
[42]Y. L. Huang, Y. Ma, R. Job, W. R. Fahrner, E. Simoen, and C. Claeys, J. Appl. Phys. **98**, 033511 (2005).
[43]See e.g., R. Murray, Phys. B: Condens. Matter **170**, 115 (1991) and references therein.
[44]W. Daum, H. J. Krause, U. Reichel, and H. Ibach, Phys. Scr. **1993**, 513.
[45]R. B. Laughlin, J. D. Joannopoulos, and D. J. Chadi, Phys. Rev. B **21**, 5733 (1980).
[46]N. M. Johnson, D. J. Bartelink, and M. Schulz, in *The Physics of SiO_2 and its Interfaces*, edited by S. Pantelides (Pergamon, New York, 1978), pp. 421–427.
[47]L. Dobaczewski, S. Bernardini, P. Kruszewski, P. K. Hurley, V. P. Markevich, I. D. Hawkins, and A. R. Peaker, Appl. Phys. Lett. **92**, 242104 (2008).
[48]E. Cartier, J. H. Stathis, and D. A. Buchanan, Appl. Phys. Lett. **63**, 1510 (1993).
[49]P. Wagner, C. Holm, E. Sirtl, R. Oeder, and W. Zulehner, Adv. Solid State Phys. **24**, 191 (1984).
[50]P. Wagner and J. Hage, Appl. Phys. A **49**, 123 (1989).
[51]G. D. Watkins and J. W. Corbett, Phys. Rev. **121**, 1001 (1961).
[52]E. V. Monakhov and B. G. Svensson, *Silicon, Germanium, and Their Alloys: Growth, Defects, Impurities, and Nanocrystals* (CRC Press, Miami, 2014), pp. 245–276.
[53]J. H. Bleka, H. Malmbekk, E. V. Monakhov, and B. G. Svensson, Phys. Rev. B **85**, 085210 (2012).
[54]J. Bang and K. J. Chang, Appl. Phys. Lett. **92**, 132109 (2008).